

Bow Echo Sensitivity to Ambient Moisture and Cold Pool Strength

RICHARD P. JAMES, PAUL M. MARKOWSKI, AND J. MICHAEL FRITSCH

Department of Meteorology, The Pennsylvania State University, University Park, Pennsylvania

(Manuscript received 16 December 2004, in final form 22 June 2005)

ABSTRACT

Bow echo development within quasi-linear convective systems is investigated using a storm-scale numerical model. A strong sensitivity to the ambient water vapor mixing ratio is demonstrated. Relatively dry conditions at low and midlevels favor intense cold-air production and strong cold pool development, leading to upshear-tilted, “slab-like” convection for various magnitudes of convective available potential energy (CAPE) and low-level shear. High relative humidity in the environment tends to reduce the rate of production of cold air, leading to weak cold pools and downshear-tilted convective systems, with primarily cell-scale three-dimensionality in the convective region. At intermediate moisture contents, long-lived, coherent bowing segments are generated within the convective line. In general, the scale of the coherent three-dimensional structures increases with increasing cold pool strength.

The bowing lines are characterized in their developing and mature stages by segments of the convective line measuring 15–40 km in length over which the cold pool is much stronger than at other locations along the line. The growth of bow echo structures within a linear convective system appears to depend critically on the local strengthening of the cold pool to the extent that the convection becomes *locally* upshear tilted. A positive feedback process is thereby initiated, allowing the intensification of the bow echo. If the environment favors an excessively strong cold pool, however, the entire line becomes uniformly upshear tilted relatively quickly, and the along-line heterogeneity of the bowing line is lost.

1. Introduction

The bow echo has been identified as one of the more common forms of convective organization over the United States and is often responsible for severe wind damage (Klimowski et al. 2003). Observational studies, beginning with Fujita (1978), have shown that bow echoes consist of a bowing segment of intense convection, with a concentrated rear inflow directed toward the apex of the bow at low to midlevels behind the gust front (Weisman 2001). Bow echo organization can arise from the growth and intensification of an isolated cell or as part of a larger squall line.

Several studies have investigated the environmental conditions conducive to derecho events, which consist of “a family of downburst clusters” (Johns and Hirt 1987) and are usually associated with bow echoes (Weisman 2001; Coniglio et al. 2004). Johns and Hirt (1987) found that warm-season derecho environments typically exhibited extreme potential instability and

high low-level dewpoints associated with the pooling of low-level moisture along a quasi-stationary thermal boundary. Wind speeds at 500 hPa were relatively strong for the warm season, averaging about 20 m s^{-1} . Johns et al. (1990) found that for 14 intense summertime derechos, the surface–700-hPa shear vector magnitudes averaged about 15 m s^{-1} . However, Evans and Doswell (2001) showed that derechos may occur throughout the year under a wide range of environmental conditions. Observed wind shear magnitudes varied widely, and derecho events that occurred in conjunction with strong synoptic-scale forcing often did not require large convective available potential energy (CAPE).

Numerical modeling has been used as a tool to study the subset of bow echoes that occurs under weak upper-level forcing with substantial potential buoyant energy (Weisman 1993; Skamarock et al. 1994; Weisman and Davis 1998). Bow echo convection arising within strongly forced environments with little or no CAPE is less amenable to idealized simulations, and, to the authors’ knowledge, has been reproduced only by Bernardet and Cotton (1998). In that study, a nocturnal derecho-producing system matured in the presence of a very

Corresponding author address: Mr. Richard P. James, 503 Walker Building, University Park, PA 16802.
E-mail: rpj105@earthlink.net

stable boundary layer; the convection was elevated in nature and was therefore dynamically distinct from the surface-based high-CAPE convection that has been studied in most bow echo modeling work. Weisman (1993) found that numerically simulated bow echo convection was favored under conditions of strong instability ($>2000 \text{ J kg}^{-1}$) and strong low-level shear ($>20 \text{ m s}^{-1}$ over the lowest 2.5–5 km). Weaker shear produced highly upshear tilted convective systems, with weak, disorganized cells rearward of the gust front. Strong shear in combination with relatively weak CAPE tended to produce lines of strong, isolated cells scattered along the gust front.

The shear magnitudes required to generate bow echo convection in the aforementioned idealized modeling studies have been the subject of some concern (Evans and Doswell 2001; Coniglio et al. 2004), because the observations indicate that weakly forced, high-CAPE bow echoes usually occur with low-level (0–5 km) shear magnitudes less than 20 m s^{-1} . A possible explanation for at least some of the discrepancy between the modeling and observational results was suggested by James et al. (2005), who noted that idealized models usually employ a free-slip lower boundary condition [see also Weisman (1993) for a brief discussion of the influence of the free-slip condition]. In observational studies, the wind magnitude at the bottom of the low-level shear layer is taken as the 10-m wind speed, which is reduced by friction from the wind speed a few hundred meters above the ground. Consequently, the measured low-level shear is reduced from the value that it would assume above a free-slip boundary. The results of James et al. (2005) show that the difference between the surface wind speed and the wind speed above the surface-based friction layer is as great as 5 m s^{-1} in the preconvective environments of strong slab-like squall lines. It is possible, therefore, that the rather high shear requirements of simulated bow echoes may not be grossly inconsistent with the less extreme observed values, because of the physically differing frameworks. However, in order to accurately simulate the near-surface friction layer and thereby resolve the discrepancy, it would be necessary to use very small grid spacing near the ground. This requirement is beyond the computational resources of most studies at the present time.

The modeling results previously published in the literature have focused primarily on the sensitivity of simulated bow echoes to kinematic conditions, particularly the low-level shear magnitude, as well as the magnitude of the CAPE. The effect of differing quantities of ambient moisture has not been specifically addressed, despite the fact that observed warm-season (weakly forced) bow echoes tend to occur in conjunc-

tion with strikingly high low-level dewpoints (Johns and Hirt 1987; Johns et al. 1990). High low-level dewpoints are, of course, partly responsible for the extreme CAPE values that are often present in derecho environments. However, this paper shows that bow echo convection is highly sensitive to variations in ambient moisture even when the CAPE is held constant.

Section 2 describes the modeling framework and methodology that was used to study bow echo development within quasi-linear convective systems; results and discussion follow in section 3. Finally, section 4 summarizes the advances made in the understanding of bow echo convection.

2. Methodology

The numerical model of Bryan and Fritsch (2002) and Bryan (2002) was used to investigate bow echo sensitivity to environmental moisture. The model integrates the compressible Navier–Stokes equations using third-order Runge–Kutta time differencing and sixth-order spatial derivatives for the advection terms. The model setup was the same as that of James et al. (2005), with a horizontal grid spacing of 500 m and a vertical grid spacing of 200 m below 5 km, increasing to 500 m above 8.5 km (see the appendix for details of the model setup). Ice microphysics was used in all simulations. The only differences from the modeling framework of James et al. (2005) were that the along-line domain dimension was increased to 120 km, in order to accommodate the development of coherent three-dimensional features on a 20–60-km scale, and the across-line domain dimension was reduced to 360 km.

The model was initialized with a line of warm bubbles with a spacing of 20 km (see the appendix). This initialization method is very similar to that used by Skamarock et al. (1994) and Weisman and Davis (1998), except that an effectively infinite line of cells is used here, with periodic boundary conditions in the along-line direction. The periodic boundary conditions preclude the development of system-scale three-dimensionality, allowing the investigation to focus narrowly on the growth of bowing segments within quasi-linear convective systems. When open boundary conditions were employed in one bow echo simulation as a sensitivity experiment, the results were qualitatively similar, although the bowing features emerged more rapidly and attained a larger scale within 6 h than in the corresponding simulation with periodic boundary conditions.

An analytic approach was used to generate base-state temperature and moisture profiles, in a similar manner to McCaul and Weisman (2001). The technique was complicated here by the fact that low-level moisture

was not held constant, and consequently the lifting condensation level (LCL) differed from sounding to sounding. The primary objective was to modify the low-level mixing ratios in a systematic manner while maintaining CAPE; this was accomplished by establishing a fixed “mixing layer” depth (1100 m when the CAPE was 4600 J kg^{-1}), with a fixed temperature, pressure, and relative humidity at the top of the mixing layer (291 K, 880 hPa, and 95%, respectively, for CAPE of 4600 J kg^{-1}). The potential temperature lapse rate in the mixing layer was then held constant at -1 K km^{-1} , but the lapse rate of water vapor mixing ratio was varied from 0 to $5.0 \text{ g kg}^{-1} \text{ km}^{-1}$. The surface-level dewpoints in the resulting soundings were in the range $19^\circ\text{--}24^\circ\text{C}$, which is consistent with observed dewpoints in derecho environments. For example, Bentley et al. (2000) showed that dewpoints in the initiation region of southeastward-moving derecho events in the north-central plains averaged 19°C , and dewpoints of $20^\circ\text{--}25^\circ\text{C}$ were found along and south of the derecho paths. Northeastward-moving derechos occurred in association with slightly lower dewpoints of $18^\circ\text{--}22^\circ\text{C}$. Johns and Hirt (1987) reported that, on average, the highest surface dewpoints associated with summertime derechos were $23^\circ\text{--}26^\circ\text{C}$.

Above the mixing-layer top, the distribution of buoyancy of a saturated parcel lifted pseudoadiabatically from the mixing-layer top was described by

$$b(z') = A \frac{m^2}{H^2} z' \exp\left(-\frac{mz'}{H}\right) - Bz'^3, \quad (1)$$

where A and B are parameters to be defined below, H is the vertical scale, m is the profile compression parameter, and z' is the height above the mixed-layer top. The second term involving the cube of the height was introduced in order to obtain a sharp cutoff to the buoyancy at the equilibrium level, as opposed to an asymptotic approach to zero in the McCaul and Weisman (2001) analytic profile. The constraint that the buoyancy is zero at the height $z' = z_{\text{EL}}$ (the equilibrium level), and knowing that the integral of the buoyancy from $z' = 0$ to $z' = z_{\text{EL}}$ is equal to the CAPE, allows the following relations to be derived:

$$A = \frac{E}{\left[1 - \left(1 + \frac{mz_{\text{EL}}}{H} + \frac{m^2 z_{\text{EL}}^2}{4H^2}\right) \exp\left(\frac{-mz_{\text{EL}}}{H}\right)\right]}, \quad (2)$$

and

$$B = \frac{Am^2}{H^2 z_{\text{EL}}^2} \exp\left(\frac{-mz_{\text{EL}}}{H}\right), \quad (3)$$

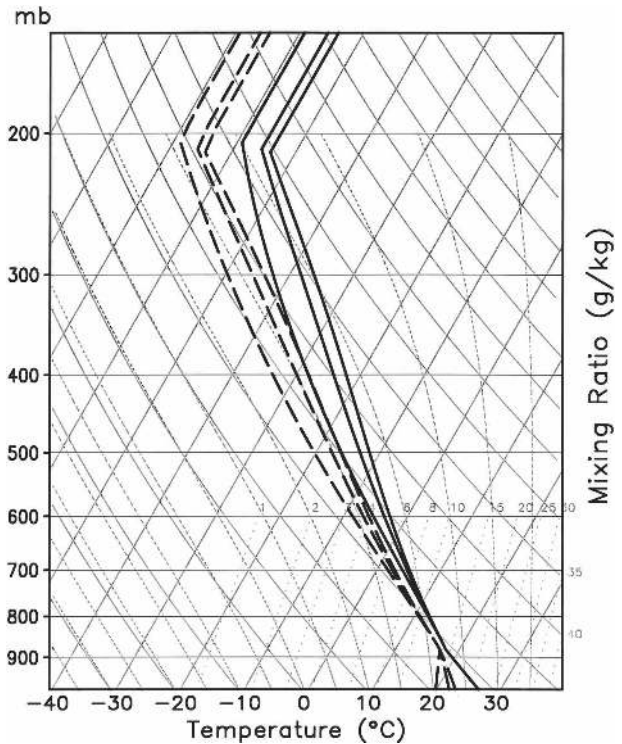


FIG. 1. Skew T -log p diagrams of three soundings with 4600 J kg^{-1} of CAPE and low-level mixing ratio lapse rates of 1, 3, and $4 \text{ g kg}^{-1} \text{ km}^{-1}$. The soundings can be distinguished by noting that a larger low-level mixing ratio lapse rate corresponds to a moister mixed layer, as well as to higher temperatures and mixing ratios above the mixed layer top.

where E is the CAPE for a saturated parcel lifted from the top of the mixing layer. In all the soundings, the scale height H was 12.75 km , and the equilibrium height z_{EL} was 12.9 km (14 km above ground). The parameter E was adjusted to maintain the total CAPE, which was calculated using the most unstable parcel. Therefore, when moisture was added to the low levels, the parameter E was reduced to maintain the total CAPE. The parameter m was chosen initially by trial and error to maximize buoyancy in the midtroposphere. Thereafter, m was adjusted for each sounding in order to maintain the vertical gradient of buoyancy at the top of the mixing layer.

The mixing ratio profile above the mixing layer top was calculated by using the same relative humidity profile in each sounding; the relative humidity R was required to diminish from 0.95 at the mixing layer top to 0.25 at the tropopause level (12 km) according to the following relation:

$$R(z) = \alpha - \beta \left(\frac{z}{z_{\text{trop}}}\right)^{1.25}, \quad (4)$$

TABLE 1. Sounding parameters for the soundings depicted in Fig. 1.

Low-level lapse rate of mixing ratio	1 g kg ⁻¹ km ⁻¹	3 g kg ⁻¹ km ⁻¹	4 g kg ⁻¹ km ⁻¹
Parameter <i>m</i>	-0.375	0.716	1.319
Parameter <i>E</i>	5115 J kg ⁻¹	3494 J kg ⁻¹	2740 J kg ⁻¹
CAPE	4600 J kg ⁻¹	4600 J kg ⁻¹	4600 J kg ⁻¹
Convective inhibition (CIN)	13 J kg ⁻¹	3 J kg ⁻¹	1 J kg ⁻¹
LCL	945 m (896 hPa)	680 m (924 hPa)	560 m (937 hPa)
LFC	1170 m (872 hPa)	745 m (916 hPa)	595 m (932 hPa)
Equilibrium level	12 688 m (176 hPa)	12 838 m (176 hPa)	12 925 m (175 hPa)

where z_{trop} is the tropopause height, and α and β are chosen according to the height of the mixing-layer top. Owing to the need to conserve CAPE, the soundings with relatively high low-level moisture also exhibited high midlevel moisture, and soundings that were relatively dry at low levels were also dry at mid-levels.

In summary, each constant-CAPE set of soundings had variable lapse rates of mixing ratio within the mixing layer and variable temperature and mixing ratio aloft, but identical total CAPE and the same vertical gradient of buoyancy at the top of the mixing layer. A tropopause was included at 12 km above ground in all soundings. The method is illustrated by showing in Fig. 1 three soundings with CAPE of 4600 J kg⁻¹; various sounding parameters are recorded in Table 1 (note that the equilibrium level in the final soundings is lower than 14 km owing to the inclusion of the tropopause).

Three sets of simulations were performed with CAPE of 4600 J kg⁻¹ in order to reproduce the extremely unstable environment in which many weakly forced, warm-season bow echoes occur. The wind vectors were directed perpendicular to the line of initialization at all levels, and wind shear was confined to the lowest 2.5 km. Simulations were carried out with 0–2.5-km wind shear magnitudes of 16, 20, and 24 m s⁻¹ (Fig. 2) leading to bulk Richardson numbers of 93, 59, and 41, respectively; for each shear value, the low-level moisture was systematically varied as described above. It is recognized that many derechos occur in wind shear profiles that are both deeper and considerably weaker in the low levels (Evans and Doswell 2001). The choice of wind shear profiles for this study was made in order to most readily obtain simulated bow echo convection, and to conform to previous modeling studies that have employed very similar shear profiles (e.g., Weisman 1993; Weisman and Davis 1998). Another set of simulations was performed with CAPE of 2300 J kg⁻¹ and 0–2.5-km shear of 20 m s⁻¹ in order to assess the robustness of the conclusions reached from the high-CAPE simulations. All of the simulations had a 6-h integration length.

3. Results and discussion

All of the simulations produced long-lived convective systems organized in a linear manner parallel to the line of initialization. Early in the simulations the convection was upright or downshear tilted, but when the sounding contained relatively little moisture, the systems became strongly upshear tilted by the mature stage (4–5 h). The transition to an upshear-tilted system occurred in these cases because the cold pool became very strong relative to the ambient wind shear, as will be demonstrated in detail later. When the cold pool remained weak, the convection remained upright or downshear tilted through the 6-h duration of the simulations. In general, then, the overall two-dimensional evolution was consistent with previous conceptual models of squall-line evolution (Weisman et al. 1988; Lafore and Moncrieff 1989).

The sensitivity of the cold pool strength to the ambient moisture content was remarkably strong. For each shear profile and CAPE value, a striking transition was observed as the environmental moisture content was systematically altered; this transition is illus-

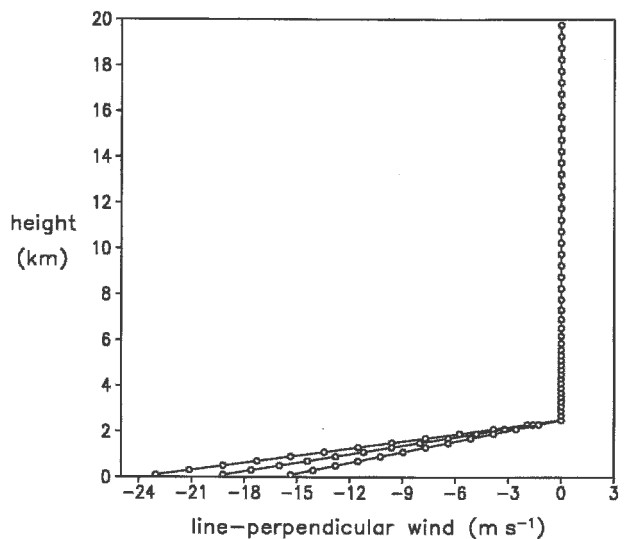


FIG. 2. Initial wind profiles used in the simulations.

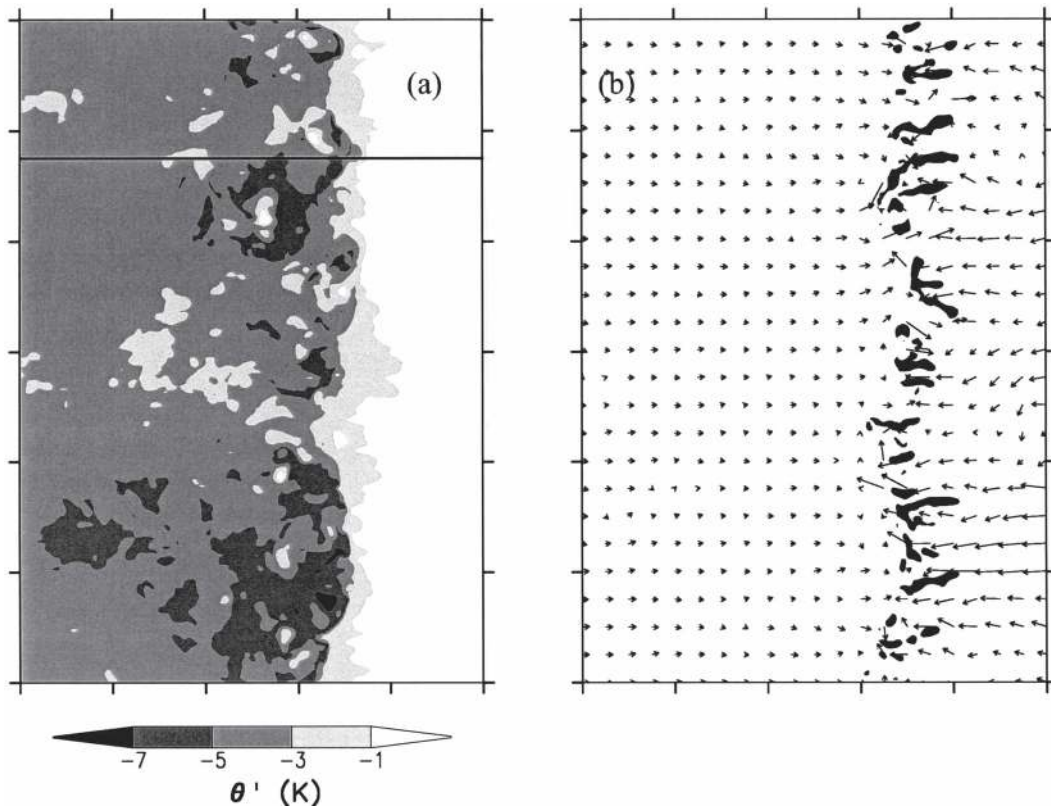


FIG. 3. (a) Potential temperature perturbation (K) at 100 m above ground (AGL), and (b) vertical velocity (shaded above 6 m s^{-1}) and approximate line-relative wind (arrows) at 3 km AGL at 6 h for the simulation with 4600 J kg^{-1} of CAPE, 0–2.5-km shear of 24 m s^{-1} , and low-level mixing ratio lapse rate of $4 \text{ g kg}^{-1} \text{ km}^{-1}$. Tick marks indicate 20-km distances. An arrow length of 10 km represents a wind speed of 25 m s^{-1} . The horizontal line in (a) indicates the location of the cross section in Fig. 4.

trated in Figs. 3–8. At high moisture levels (relative to other soundings with the same shear and CAPE), the convective system consisted of a line of strong but isolated cells above the leading edge of a weak cold pool (e.g., Figs. 3 and 4). The two-dimensional “slab” lifting that is often found above a continuous gust front (James et al. 2005) was weak or nonexistent in these cases, with cell-scale three-dimensionality dominating the convective mode at all levels. At relatively low moisture levels (e.g., when the water vapor profile was approximately well mixed in the mixing layer), the cold pool was very strong and homogeneous, and intense slab lifting occurred above the gust front (e.g., Figs. 7 and 8). In these simulations, short-lived bowing segments sometimes occurred, but long-lived coherent bow structures did not develop. These “slabular” convective systems were highly upshear tilted, but the convection was nevertheless strong and persistent along the leading edge.

At intermediate quantities of low-level (and mid-level) moisture, the bow echo mode of convection was

observed. In these systems, the convection was at first downshear tilted in combination with a weak cold pool. After 3–5 h, the cold pool became suddenly much stronger *locally* along the squall line, while remaining relatively weak at other locations. In response to the locally stronger and deeper cold pool, the gust front began to surge out, and the convection assumed a bowing shape along the portion of the cold pool that was stronger (e.g., Figs. 5 and 6). In conjunction with the bowing of the leading-edge convection, a concentrated zone of rear inflow developed behind the bow and penetrated to the apex of the bow. A pair of vortices was observed on either side of the rear inflow jet associated with each bowing segment. The development of these bow echo features was therefore consistent with previous observational and modeling studies (Przybylinski 1995; Weisman 1993, 2001).

The “spectrum” of convective modes described above, dependent on ambient moisture, was observed for all the shear magnitudes that were tested, and for both moderate (2300 J kg^{-1}) and very high (4600 J kg^{-1})

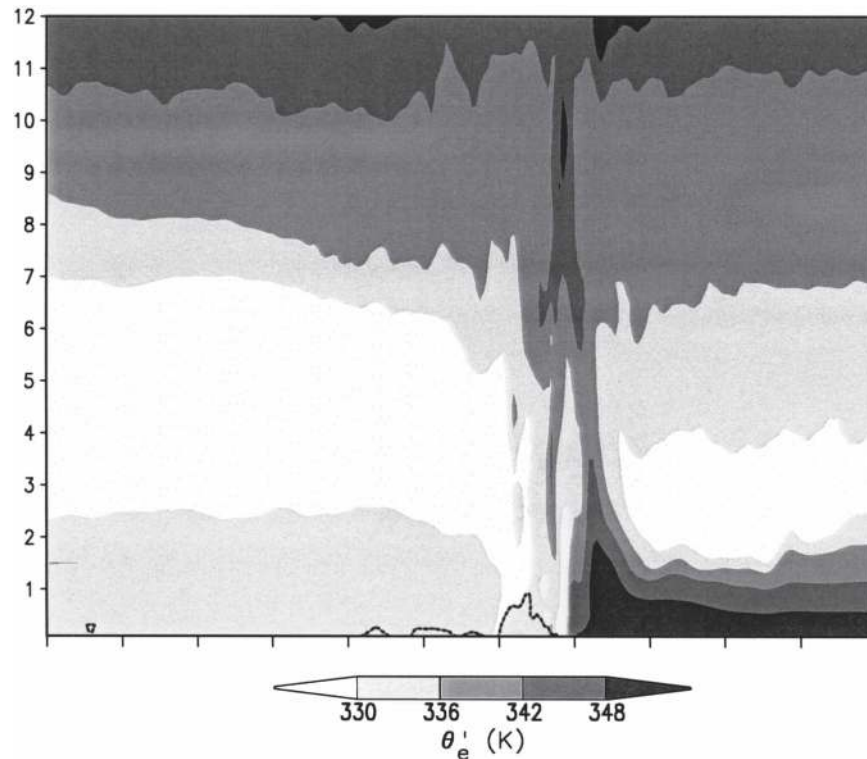


FIG. 4. Vertical cross section through the simulation with 4600 J kg^{-1} of CAPE, 0–2.5-km shear of 24 m s^{-1} , and low-level mixing ratio lapse rate of $4 \text{ g kg}^{-1} \text{ km}^{-1}$ at 6 h, at the location marked in Fig. 3a. Tick marks along the abscissa indicate 10-km distances; the ordinate is labeled in km above ground. Equivalent potential temperature (K) is shaded; the dotted line indicates the -4 K perturbation potential temperature line.

CAPE. The bow echo convection was strongest and most clearly defined for the high-shear, high-CAPE environment, as might be expected (Weisman 1993). Nevertheless, a structure involving bowing segments (i.e., a bow echo mode) was observed as an intermediate mode between the downshear-tilted, cell-dominated squall line, and the upshear-tilted, slabular squall line for *all* the shear and CAPE magnitudes, indicating that the dependence of convective mode on environmental moisture is consistent within the parameter range tested.

The lines in which bow echo segments occurred were characterized by the development of significant cold pool inhomogeneities along the line on a scale of 15–40 km. Indeed, the localized strengthening of the cold pool appears to have been the trigger that initiated the development of bow echo structures. To quantitatively investigate the cold pool inhomogeneities, the cold pool strength C (Weisman 1992) was calculated at each row of grid points intersecting the line, as follows:

$$C^2 = -2g \int_0^D \left(\frac{\theta_p - \theta_{p0}}{\theta_{p0}} \right) dz, \quad (5)$$

where D is the depth of the cold pool and θ_p is the density potential temperature (Emanuel 1994). The depth of the cold pool was defined as the upper limit of the -1 K potential temperature perturbation, and C was averaged over a 10-km distance behind the gust front. Figures 9–11 show the integrated cold pool strength C as a function of along-line position for three simulations at 4 and 6 h, along with the ratio $C/\Delta U$, where ΔU is the 0–2.5-km shear magnitude. The ratio $C/\Delta U$ is a measure of the relative strengths of the circulation associated with the cold pool and the circulation associated with the low-level shear; values substantially less than one tend to be associated with downshear-tilted convection, while values much greater than one occur in conjunction with upshear-tilted convection (Rotunno et al. 1988). Figure 9 illustrates the dominance of the shear magnitude over the cold pool strength in the high-CAPE, high-shear simulation with very moist low levels (low-level mixing ratio lapse rate of $4 \text{ g kg}^{-1} \text{ km}^{-1}$). The cold pool strength did not increase significantly between 4 and 6 h, and at no location did the cold pool become strong enough to initiate a local transition to an upshear-tilted mode.

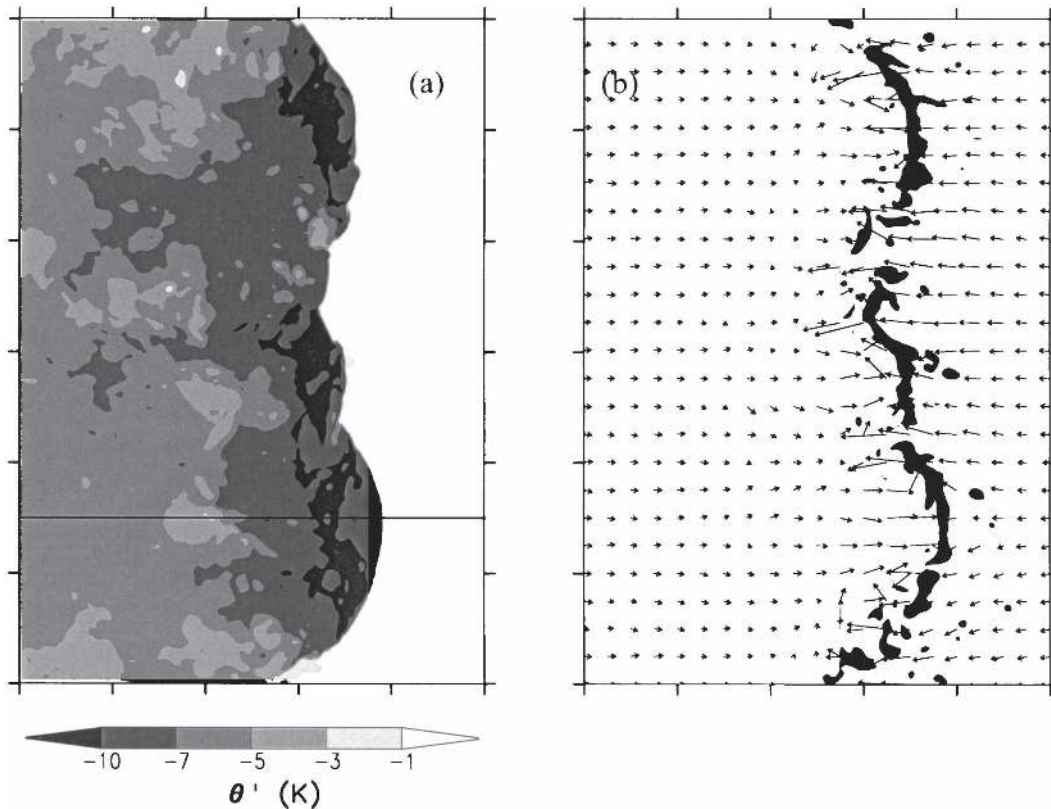


FIG. 5. As in Fig. 3, but for the simulation with a low-level mixing ratio lapse rate of $3 \text{ g kg}^{-1} \text{ km}^{-1}$; the horizontal line in (a) indicates the location of the cross section in Fig. 6.

In contrast, a modest decrease in the ambient moisture (low-level mixing ratio lapse rate of $3 \text{ g kg}^{-1} \text{ km}^{-1}$) caused the cold pool to strengthen sufficiently to allow a cold pool–shear balance, and eventually cold pool dominance, at certain locations along the line (Fig. 10). The locations at which the cold pool is strongest correspond to the bowing segments (Fig. 5). The overall increase of cold pool strength with decreasing ambient moisture arises partly because the rate of condensate (rainwater) evaporation is sensitive to the low-level relative humidity. For the same amount of condensate falling into a subcloud layer, a drier subcloud layer will evaporate more condensate and therefore generate more cold air at low levels. Additionally, the soundings with drier midlevels exhibit lower equivalent potential temperature at midlevels, which is conducive to the formation of colder downdrafts and a stronger cold pool (Gilmore and Wicker 1998).

After a critical threshold in the cold pool strength is reached, the steadily increasing upshear tilt of the convection and the further intensification of the cold pool appear to be a self-reinforcing process as envisioned by Szeto and Cho (1994). The simulations indicate that this threshold corresponds approximately

to the cold pool–shear balance condition; consequently, the development of bowing segments begins after the cold pool strengthens enough locally to balance the shear. The locally intense cold pool and upshear-tilted convection favor the local strengthening of rear inflow, which is a crucial component of the bow echo feature. As the rear inflow develops and transports air cooled by evaporation and melting toward the bow echo apex at increasing rates, the cold pool strengthens yet further locally. The bow echo segment is generated, therefore, by a positive feedback mechanism contingent on the *local* strengthening of the cold pool to the extent that the convection becomes locally upshear tilted.

It is not immediately apparent why the bowing segments develop on a preferred scale of 15–40 km. The inhomogeneities in the cold pool strength develop initially on a smaller scale (2–10 km) associated with random strengthening or weakening of the convection at certain locations along the line. It appears that the subsequent upscale growth of the intensifying bowing features is related to the lateral spreading of the locally intense cold pool, owing to an increased rate of production of cold air in the vicinity of the bow. This pro-

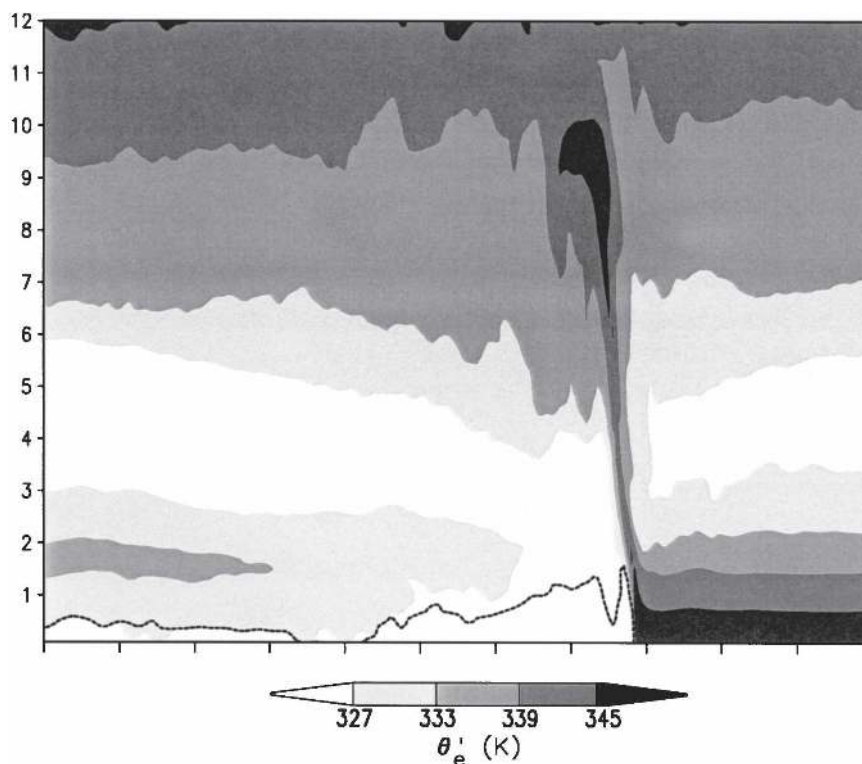


FIG. 6. As in Fig. 4, but for the simulation with a low-level mixing ratio lapse rate of $3 \text{ g kg}^{-1} \text{ km}^{-1}$, at the location marked in Fig. 5a.

cess of cold pool spreading and upscale growth is illustrated in Fig. 12. The scale of the simulated bowing segments is on the smaller end of observed bow echo sizes, but is within the range of observed scales. For example, Johns (1993) indicates that bow-shaped echoes range in scale from less than 15 km to more than 150 km; Coniglio et al. (2004) suggest a range of scales of 10–300 km; and Weisman (2001) states that the most severe bow echoes typically occur on scales of 40–120 km. Further investigation of the scale dependence of bow echoes within quasi-linear convective systems is required.

The soundings that are relatively dry are conducive to very strong cold pool development. Figure 11 shows that the cold pool strength overwhelms the low-level shear at most locations along the line by 4 h into the squall-line evolution. By 6 h, the cold pool is very strong and quite homogeneous along the line. Clearly, the dynamical heterogeneity of the bowing lines is no longer present, so that the convection becomes upshear tilted everywhere along the line. This mode of squall-line development, being dominated by the cold pool in the mature stage, is akin to the strongly “slabular” line of James et al. (2005).

It is of interest to consider why the simulations

with very strong cold pool development (Figs. 7 and 11) are unable to generate bow echo convection. One might expect that bowing segments would arise in a similar manner to the bow echo simulation, but at an earlier time because of the accelerated cold pool growth. It appears that this does not occur because the very rapid production of cold air causes the cold pool to overwhelm the shear *everywhere* along the line, thereby eliminating the dynamical heterogeneity that persists in the bowing lines. Thus, when the cold pool strengthens rapidly everywhere, the time period during which the cold pool overwhelms the shear locally *while not doing so elsewhere* is relatively short. This fact is illustrated in Fig. 13, which shows the evolution in time of the fraction of points along the line at which the ratio $C/\Delta U$ is greater than one, for the two simulations depicted in Figs. 5 and 7. The cold pool in the slab-like simulation (i.e., with low low-level moisture) strengthens rapidly enough that the fraction of points at which the cold pool dominates increases from 0.07 to 0.81 in 1 h. In the bow echo simulation, an increase from 0.08 to 0.76 takes 2 h to occur. Thus, for the intermediate low-level moisture values, the time over which the profound dynamical differences are maintained over different portions of the

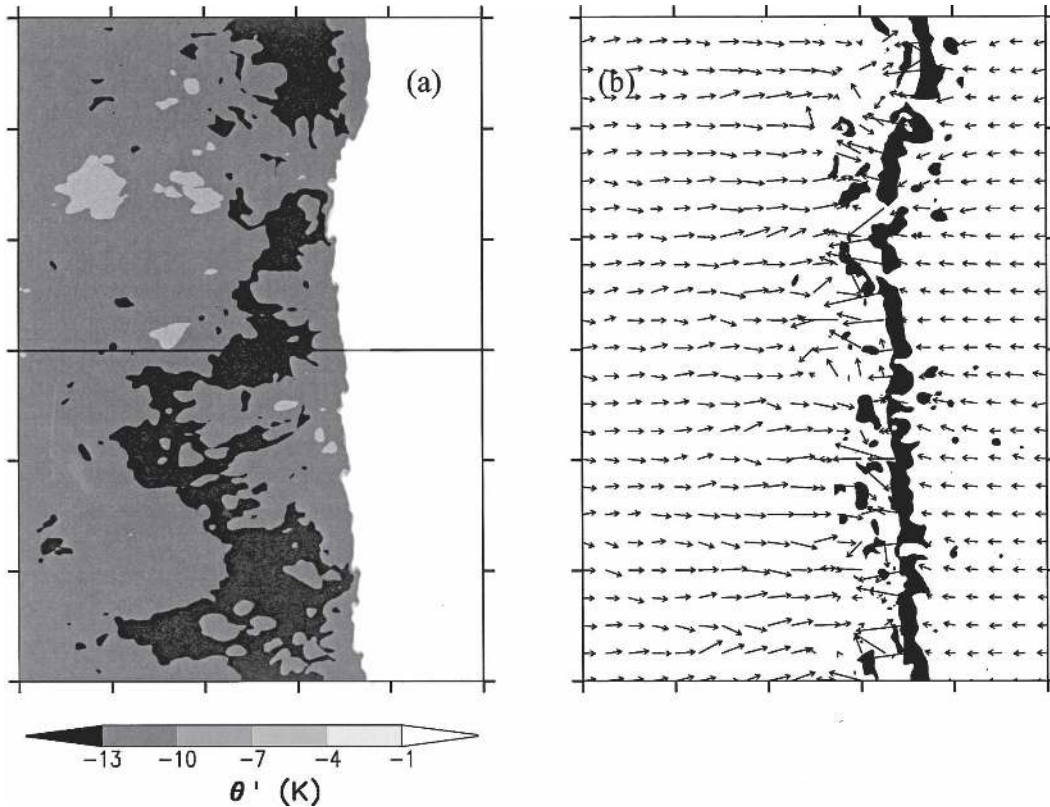


FIG. 7. As in Fig. 3, but for the simulation with a low-level mixing ratio lapse rate of $1 \text{ g kg}^{-1} \text{ km}^{-1}$; the horizontal line in (a) indicates the location of the cross section in Fig. 8.

line is much longer, allowing pronounced bowing to occur.

4. Conclusions

The numerical experiments described herein suggest that the mode of linearly organized convection is very sensitive to the quantity of water vapor in the ambient environment. A relatively dry environment, combined with sufficient CAPE and shear to sustain a convective system, favors a strong cold pool that quickly overwhelms the ambient shear and causes the convection to assume a “slabular” mode. This result is consistent with the single-cell simulations of McCaul and Cohen (2002), who found that a higher LCL (and consequently a lower mean mixed-layer relative humidity) is conducive to outflow dominance. Similarly, Gilmore and Wicker (1998) reported that dry air at midtropospheric levels favors a strong, cold low-level outflow. In contrast, excessive moisture at low to midlevels hinders the development of the cold pool (even for very large CAPE) to such an extent that the convection remains cell dominated and upright or downshear tilted. Extreme shear is not required in order to obtain a down-

shear-tilted squall line; the primary requirement is simply that the cold pool remains weak relative to the shear.

The results indicate that long-lived, coherent bowing segments are most likely to develop within a quasi-linear convective system when the ambient moisture falls in a range that permits an intermediate strength of cold pool. The important feature of the bow echo development appears to be that the cold pool overwhelms the low-level shear, *but only locally*. If the cold pool is locally strong enough, the convection tilts upshear and initiates a positive feedback process that causes the growth and intensification of the bowing segment. However, if the rate of production of cold air is very great everywhere along the line, the convection quickly becomes upshear tilted everywhere. In these “slabular” systems, the along-line heterogeneity of the cold pool does not persist long enough to permit substantial bowing in the line.

It is important to note that cold pool strength depends on other environmental factors than just the ambient moisture, and therefore bow echo sensitivity likely exists for many other parameters. The purpose of this paper is not to exhaustively investigate bow echo

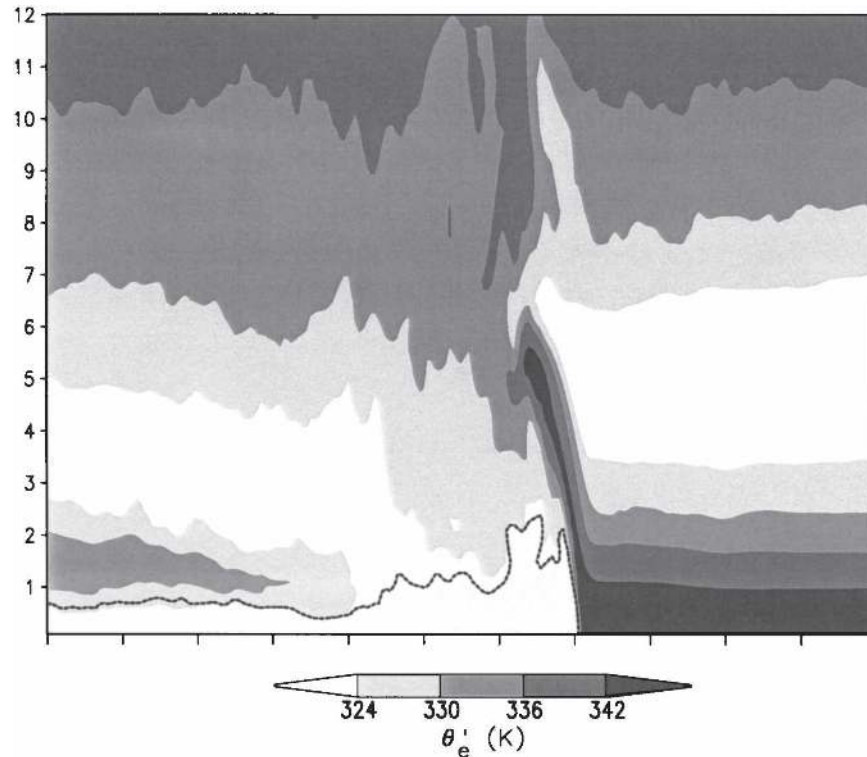


FIG. 8. As in Fig. 4, but for the simulation with a low-level mixing ratio lapse rate of $1 \text{ g kg}^{-1} \text{ km}^{-1}$, at the location marked in Fig. 7a.

sensitivities, but to demonstrate the profound effect of subtle alterations to the ambient moisture, and to show that the bowing convective line may be regarded as an intermediate convective mode, between the cell-dominated downshear-tilted squall line, and the slab-like upshear-tilted squall line. The spectrum of modes surrounding the bow echo is likely to exist across the range of any parameter that significantly affects the rate of production of cold air and the cold pool strength.

In general, it appears that the scale of the coherent three-dimensional features within a squall line is closely related to the cold pool strength, with stronger cold pools favoring larger scales. When the cold pool is weak, cell-scale three-dimensionality dominates; this result is consistent with the work of James et al. (2005), who found that lines of discrete cells are favored when the production of low-level cold air is too weak to permit the merging of the cold pools associated with individual cells. It seems likely, then, that squall lines forming within environments with relatively high humidity may have an enhanced likelihood of containing embedded rotating storms. At the opposite end of the dimensionality spectrum is the “slabular” line; the bow echo consists of an intermediate scale of three-dimensionality.

The results presented here expand on previously published investigations of bow echo sensitivity to environmental conditions. Weisman (1993) argued that a necessary condition for bow echo generation is that minimum thresholds of CAPE and shear be satisfied. The experimentation reported here did not attempt to confirm these requirements, although bowing convection was obtained for 0–2.5-km shear values of 16 m s^{-1} , which is slightly lower than the minimum threshold (20 m s^{-1}) of Weisman (1993). However, detailed comparison between the results of Weisman (1993) and the present simulations is complicated by the fact that the initiation procedure of Weisman (1993) used a single warm bubble, which is less favorable for the development of quasi-two-dimensional (“slabular”) systems. The simulations reported here, which focus specifically on bow echoes within convective lines, show that large CAPE and shear may not be sufficient to generate bow echoes, if the environmental humidity is either too great or too little. The minimum thresholds of CAPE and shear thus constitute necessary, *but not sufficient*, conditions for bowing convection.

Future work should include more detailed investigation of the relative importance of variations in low-level versus midlevel moisture. Although the primary focus

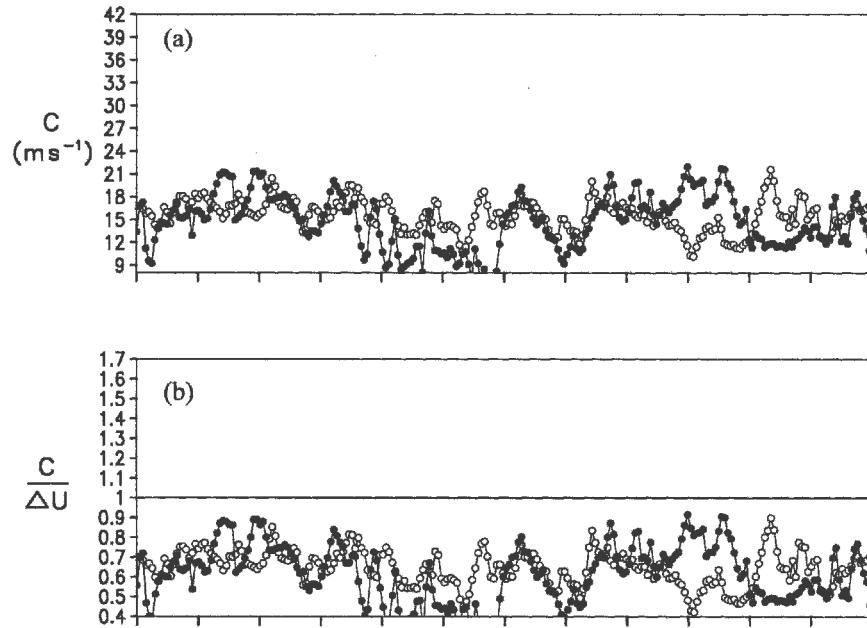


FIG. 9. (a) Cold pool strength C , and (b) cold pool-shear ratio at 4 h (open circles) and 6 h (closed circles) for the simulation with CAPE of 4600 J kg^{-1} , 0–2.5-km shear of 24 m s^{-1} , and low-level mixing ratio lapse rate of $4 \text{ g kg}^{-1} \text{ km}^{-1}$. Tick marks indicate 10-km distances in the along-line direction. The left-hand side of the diagram corresponds to the bottom (south) side of the model domain.

in the construction of our artificial soundings was the systematic variation of low-level moisture, the mixing ratio profile also changed significantly throughout the troposphere. Therefore it may be worth attempting to

isolate the effects of midlevel and low-level changes in a future study (G. H. Bryan 2005, personal communication).

It is very likely that the modeling framework used

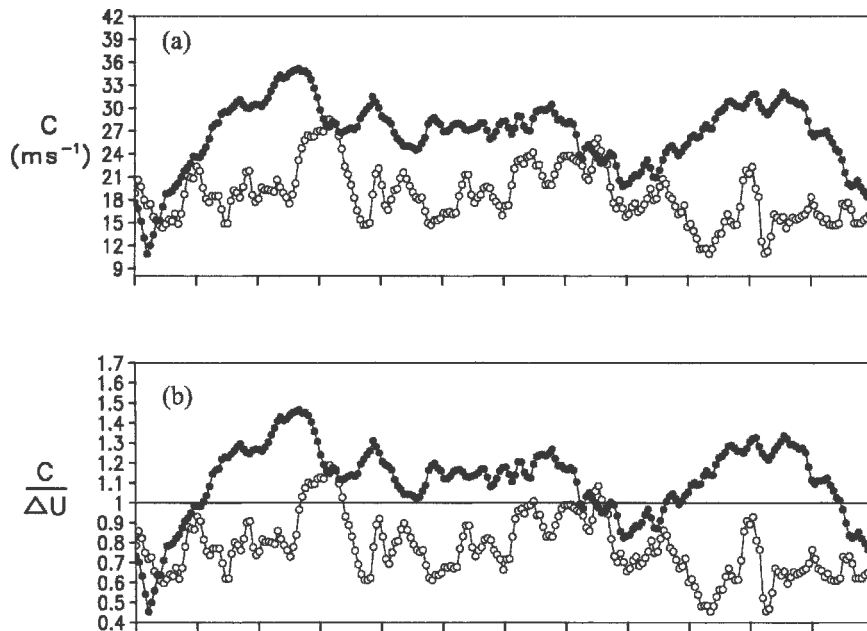


FIG. 10. As in Fig. 9, but for the simulation with a low-level mixing ratio lapse rate of $3 \text{ g kg}^{-1} \text{ km}^{-1}$.

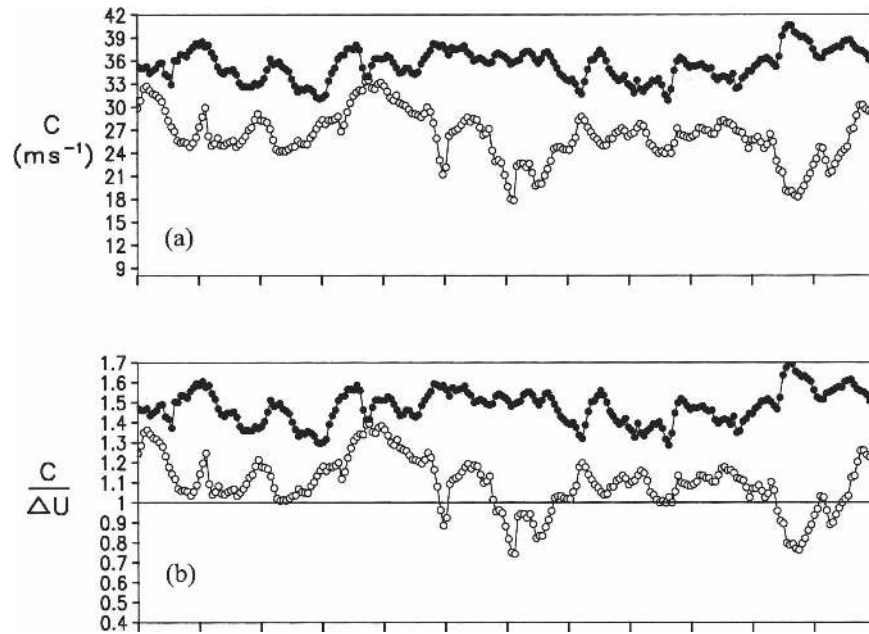


FIG. 11. As in Fig. 9, but for the simulation with a low-level mixing ratio lapse rate of $1 \text{ g kg}^{-1} \text{ km}^{-1}$.

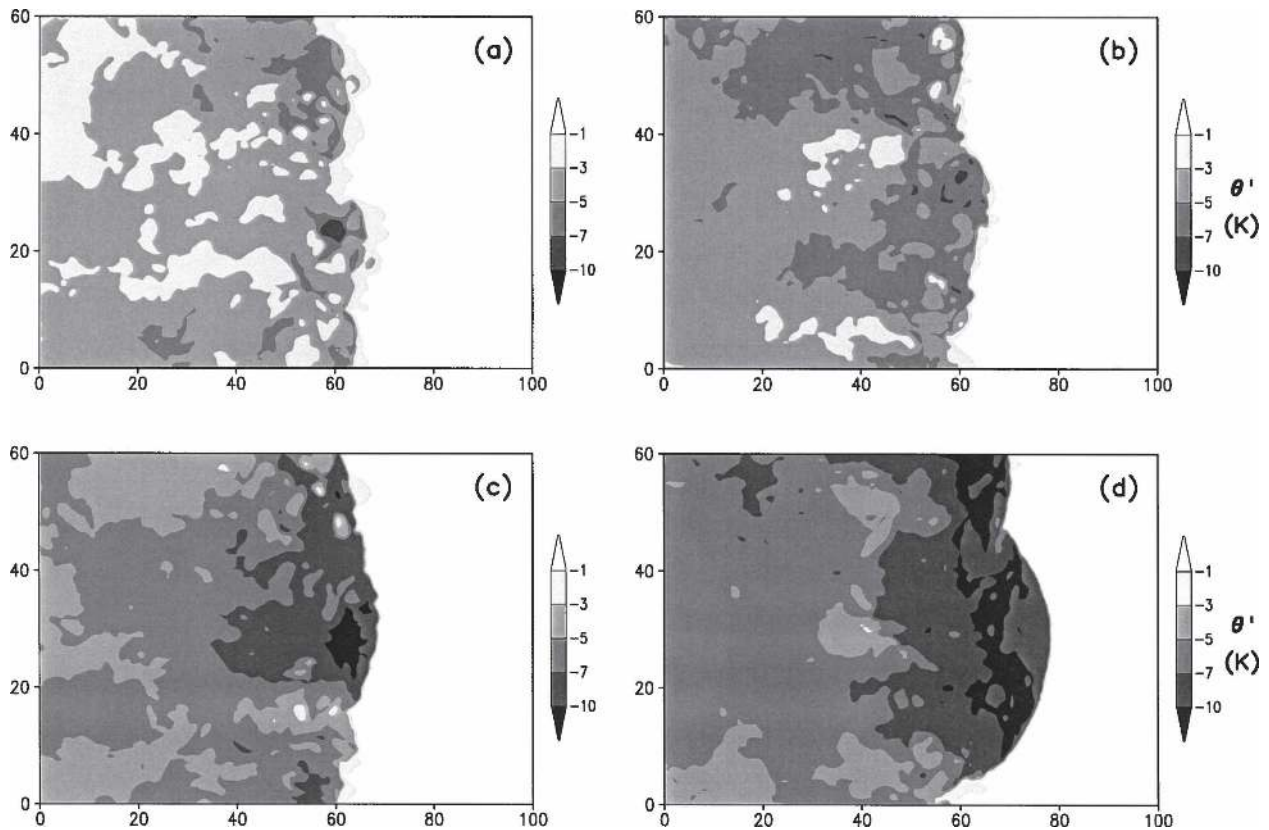


FIG. 12. Potential temperature perturbation (K) at 100 m above ground in the simulation with 4600 J kg^{-1} of CAPE, 0–2.5-km shear of 24 m s^{-1} , and low-level mixing ratio lapse rate of $3 \text{ g kg}^{-1} \text{ km}^{-1}$, at (a) 3, (b) 4, (c) 5, and (d) 6 h. The axis labels indicate distance in km.

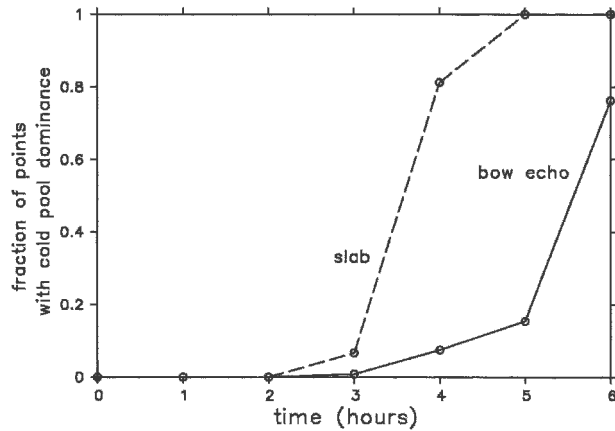


FIG. 13. Fraction of points along the line at which the cold pool–shear ratio is greater than one; data are plotted hourly through 6 h for two simulations. Each simulation had CAPE of 4600 J kg^{-1} and 0–2.5-km shear of 24 m s^{-1} . “Slab” denotes the simulation with a low-level mixing ratio lapse rate of $1 \text{ g kg}^{-1} \text{ km}^{-1}$. “Bow echo” denotes the simulation with a low-level mixing ratio lapse rate of $3 \text{ g kg}^{-1} \text{ km}^{-1}$.

here does not accurately predict the absolute moisture quantities that are needed for bow echo development within squall lines. Numerous tunable parameters in the ice microphysics and the turbulence parameterization, together with the details of the model numerics, may affect the precise dependence of the cold pool strength on environmental conditions (Bryan et al. 2004). More simulations at higher resolution, with improved microphysical schemes, are needed to assess the exact behavior of bow echo convection, and to determine the precise range of ambient moisture that favors the bow echo mode. However, the consistency of the observed trends across different CAPE and shear magnitudes suggests that, within the limited parameter range tested, the relative dependence of bow echo development and convective mode dimensionality on ambient moisture is robust.

Acknowledgments. The authors gratefully acknowledge correspondence with George Bryan on the subject

of bow echo simulations. Helpful comments were supplied by Jeremy Ross. This work was made possible by NSF Grant ATM 0133506. Computing resources were provided by the High Performance Computing Group at the Pennsylvania State University and by the Scientific Computing Division of the National Center for Atmospheric Research (NCAR). Figures were constructed using the Grid Analysis and Display System (GrADS).

APPENDIX

Model Setup Details

Various parameters pertaining to the model setup are given in Table A1.

The vertical stretching function is obtained by dividing the grid into three layers in the vertical, with the stretching of the grid confined to the middle layer. Above and below the stretching layer, the grid spacing is constant, as illustrated in Fig. A1. The total number of vertical levels, nk , is divided between the three layers as follows:

$$nk_1 = \frac{h_1}{d_1}, \tag{A1}$$

$$nk_3 = \frac{D - h_2}{d_3}, \text{ and,} \tag{A2}$$

$$nk_2 = nk - nk_1 - nk_3. \tag{A3}$$

The “full” levels, on which the vertical velocity is defined, are given by

$$z_f(k) = d_1(k - 1) \text{ for } k = 1, nk_1 + 1, \tag{A4}$$

$$z_f(k) = h_1 + d_2[c_1 + c_2(k - 1 - nk_1)d_2](k - 1 - nk_1)$$

for

$$k = nk_1 + 2, nk_2 + 1, \tag{A5}$$

where

TABLE A1. Description of various model parameters used for the simulations reported here.

Δx	500 m
Δz	Variable (200–500 m)
Vertical stretching parameters	$d_1 = 200 \text{ m}, d_3 = 500 \text{ m}, h_1 = 5 \text{ km}, h_2 = 8.5 \text{ km}, D = 20 \text{ km}$
Δt_l (long time step)	3 s
Δt_s (short time step)	0.5 s
Advection scheme	Sixth order, following Wicker and Skamarock (2002)
Artificial diffusion	Sixth order
Subgrid turbulence scheme	As in Bryan et al. (2003)
Microphysics scheme	Five condensate species including hail, following Lin et al. (1983), with modifications by the Goddard cumulus ensemble modeling group (Braun and Tao 2000)
Warm bubble initialization parameters	$\Delta\theta = 3 \text{ K}, r_h = 5 \text{ km}, r_v = 2 \text{ km}$

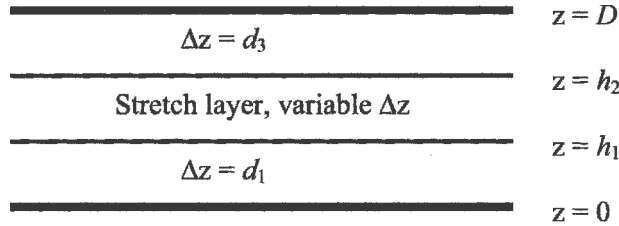


FIG. A1. Schematic diagram of the vertical arrangement of levels in the model domain of depth D . The grid spacing Δz is constant in the layers $0 < z < h_1$ and $h_2 < z < D$, but varies in the layer $h_1 < z < h_2$.

$$d_2 = \frac{h_2 - h_1}{nk_2}, \quad (\text{A6})$$

$$c_1 = \frac{d_1}{d_2} - c_2 d_2, \quad \text{and} \quad (\text{A7})$$

$$c_2 = \frac{d_2 - d_1}{d_2^2(nk_2 - 1)}; \quad (\text{A8})$$

$$z_f(k) = h_2 + d_3(k - nk_1 - nk_2 - 1) \quad \text{for} \\ k = nk_2 + 2, nk + 1. \quad (\text{A9})$$

The “half” levels, on which the scalar variables, as well as horizontal wind components, are defined, are given by

$$z_h(k) = \frac{z_f(k) + z_f(k + 1)}{2}$$

for

$$k = 1, nk. \quad (\text{A10})$$

The warm bubble initialization consists of a localized positive potential temperature perturbation introduced at the initial time. The potential temperature perturbation for each bubble is given by the following, where x_0 , y_0 , and z_0 define the location of the center of the bubble:

$$\delta\theta(x, y, z) = \Delta\Theta \cos^2\left(\frac{\pi\beta}{2}\right) \quad \text{for } \beta < 1, \quad \text{and} \\ \delta\theta(x, y, z) = 0 \quad \text{elsewhere,} \quad (\text{A11})$$

where

$$\beta = \left[\left(\frac{x - x_0}{r_h}\right)^2 + \left(\frac{y - y_0}{r_h}\right)^2 + \left(\frac{z - z_0}{r_v}\right)^2 \right]^{1/2}. \quad (\text{A12})$$

REFERENCES

Bentley, M. A., T. L. Mote, and S. F. Byrd, 2000: A synoptic climatology of derecho producing mesoscale convective systems in the north-central plains. *Int. J. Climatol.*, **20**, 1329–1349.
Bernardet, L. R., and W. R. Cotton, 1998: Multiscale evolution of

a derecho-producing mesoscale convective system. *Mon. Wea. Rev.*, **126**, 2991–3015.
Braun, S. A., and W.-K. Tao, 2000: Sensitivity of high-resolution simulations of Hurricane Bob (1991) to planetary boundary layer parameterizations. *Mon. Wea. Rev.*, **128**, 3941–3961.
Bryan, G. H., 2002: An investigation of the convective region of numerically simulated squall lines. Ph.D. thesis, The Pennsylvania State University, 181 pp.
—, and J. M. Fritsch, 2002: A benchmark simulation for moist nonhydrostatic numerical models. *Mon. Wea. Rev.*, **130**, 2917–2928.
—, J. C. Wyngaard, and J. M. Fritsch, 2003: Resolution requirements for the simulation of deep moist convection. *Mon. Wea. Rev.*, **131**, 2394–2416.
—, J. C. Knievel, and M. D. Parker, 2004: An evaluation of “RKW theory” using a model intercomparison. Preprints, *22d Conf. on Severe Local Storms*, Hyannis, MA, Amer. Meteor. Soc., CD-ROM, P6.2.
Coniglio, M. C., D. J. Stensrud, and M. B. Richman, 2004: An observational study of derecho-producing convective systems. *Wea. Forecasting*, **19**, 320–337.
Emanuel, K. A., 1994: *Atmospheric Convection*. Oxford University Press, 580 pp.
Evans, J. S., and C. A. Doswell, 2001: Examination of derecho environments using proximity soundings. *Wea. Forecasting*, **16**, 329–342.
Fujita, T. T., 1978: Manual of downburst identification for Project Nimrod. Department of Geophysical Sciences, University of Chicago Satellite and Mesometeorology Research Paper 156, 104 pp.
Gilmore, M. S., and L. J. Wicker, 1998: The influence of midtropospheric dryness on supercell morphology and evolution. *Mon. Wea. Rev.*, **126**, 943–958.
James, R. P., J. M. Fritsch, and P. M. Markowski, 2005: Environmental distinctions between cellular and slabular convective lines. *Mon. Wea. Rev.*, **133**, 2669–2691.
Johns, R. H., 1993: Meteorological conditions associated with bow echo development in convective storms. *Wea. Forecasting*, **8**, 294–299.
—, and W. D. Hirt, 1987: Derechos: Widespread convectively induced windstorms. *Wea. Forecasting*, **2**, 32–49.
—, K. W. Howard, and R. A. Maddox, 1990: Conditions associated with long-lived derechos—An examination of the large-scale environment. Preprints, *16th Conf. on Severe Local Storms*, Kananaskis Park, AB, Canada, Amer. Meteor. Soc., 408–412.
Klimowski, B. A., M. J. Bunkers, M. R. Hjelmfelt, and J. N. Covert, 2003: Severe convective windstorms over the northern High Plains of the United States. *Wea. Forecasting*, **18**, 502–519.
Lafore, J.-P., and M. W. Moncrieff, 1989: A numerical investigation of the organization and interaction of the convective and stratiform regions of tropical squall lines. *J. Atmos. Sci.*, **46**, 521–544.
Lin, Y.-L., R. D. Farley, and H. D. Orville, 1983: Bulk parameterization of the snow field in a cloud model. *J. Appl. Meteor.*, **22**, 1065–1092.
McCaul, E. W., Jr., and M. L. Weisman, 2001: The sensitivity of simulated supercell structure and intensity to variations in the shapes of environmental buoyancy and shear profiles. *Mon. Wea. Rev.*, **129**, 664–687.
—, and C. Cohen, 2002: The impact on simulated storm

- structure and intensity of variations in the mixed layer and moist layer depths. *Mon. Wea. Rev.*, **130**, 1722–1748.
- Przybylinski, R. W., 1995: The bow echo: Observations, numerical simulations, and severe weather detection methods. *Wea. Forecasting*, **10**, 203–218.
- Rotunno, R., J. B. Klemp, and M. L. Weisman, 1988: A theory for strong, long-lived squall lines. *J. Atmos. Sci.*, **45**, 463–485.
- Skamarock, W. C., M. L. Weisman, and J. B. Klemp, 1994: Three-dimensional evolution of simulated long-lived squall lines. *J. Atmos. Sci.*, **51**, 2563–2584.
- Szeto, K. K., and H.-R. Cho, 1994: A numerical investigation of squall lines. Part II: The mechanics of evolution. *J. Atmos. Sci.*, **51**, 425–433.
- Weisman, M. L., 1992: The role of convectively generated rear-inflow jets in the evolution of long-lived mesoconvective systems. *J. Atmos. Sci.*, **49**, 1826–1847.
- , 1993: The genesis of severe, long-lived bow echoes. *J. Atmos. Sci.*, **50**, 645–670.
- , 2001: Bow echoes: A tribute to T. T. Fujita. *Bull. Amer. Meteor. Soc.*, **82**, 97–116.
- , and C. A. Davis, 1998: Mechanisms for the generation of mesoscale vortices within quasi-linear convective systems. *J. Atmos. Sci.*, **55**, 2603–2622.
- , J. B. Klemp, and R. Rotunno, 1988: Structure and evolution of numerically simulated squall lines. *J. Atmos. Sci.*, **45**, 1990–2013.
- Wicker, L. J., and W. C. Skamarock, 2002: Time-splitting methods for elastic models using forward time schemes. *Mon. Wea. Rev.*, **130**, 2088–2097.